Lunar nodal tide effects on variability of sea level, temperature, and salinity in the Faroe-Shetland Channel and the Barents Sea

Harald Yndestad [a,*], William R. Turrell [b,1], Vladimir Ozhigin [c,2]

[a] Aalesund University College, N-6025 Aalesund, Norway
[b] FRS Marine Laboratory Aberdeen, PO Box 101, Victoria Road, Aberdeen AB11 9DB, Scotland
[c] Polar Research Institute of Marine Fisheries and Oceanography (PINRO), 6 Knipovich St., Mermansk 183763, Russia

ARTICLE INFO

ABSTRACT

The Faroe-Shetland Channel and the Kola Section hydrographic time-series cover a time period of more than 100 years and represent two of the longest oceanographic time-series in the world. Relationships between the temperature and salinity of Atlantic water from these two areas are examined in this paper, which also presents for the first time comparisons between them and annual mean sea levels in the region. The investigation was based on a wavelet spectrum analysis used to identify the dominant cycle periods and cycle phases in all time-series. The water-property time-series show mean variability correlated to a sub-harmonic cycle of the nodal tide of about 74 years, with an advective delay between the Faroe-Shetland Channel and the Barents Sea of about 2 years. In addition, correlations better than $R = 0.7$ were found between dominant Atlantic water temperature cycles and the 18.6-year lunar nodal tide, and better than $R = 0.4$ for the $18.6/2 = 9.3$-year lunar nodal phase tide. The correlation between the lunar nodal tides and the ocean temperature variability suggests that deterministic lunar nodal tides are important regional climate indicators that should be included when future regional climate variability is considered. The present analysis suggests that Atlantic water temperature and salinity fluctuations in the Nordic Seas are influenced by forced tidal mixing modulated by harmonics of the nodal tide and influencing the water mass characteristics at some point "down stream" from the Faroe-Shetland Channel. The effects of the modulated oceanic mixing are subsequently distributed as complex coupled lunar nodal sub-harmonic spectra in the thermohaline circulation.

© 2008 Elsevier Ltd. All rights reserved.

1. Introduction

Inflow of North Atlantic Water (NAW) passes from the North Atlantic through the Faroe-Shetland Channel and into the Norwegian Sea. The current continues north with a minor inflow to the Barents Sea. One part returns to the Greenland Sea, and one part has an inflow to the Arctic Ocean through the Fram Strait. From the Fram Strait, the current circulates in the Arctic Ocean and returns to the Greenland Sea return current (Fig. 1).

It has been well known for decades that this current has a major influence on the climate in northern Europe. To contribute to the study of regional climate variability, the temperature in the Faroe-Shetland Channel and the Kola section in the Barents Sea have been monitored for more than a 100 years; this represents two of the longest oceanographic time-series in the world. The relationship between these important time-series is

* Corresponding author. Tel.: +47 70 16 12 00; fax: +47 70 16 13 00.
  E-mail addresses: Harald.Yndestad@hials.no (H. Yndestad),
turrellb@marlab.ac.uk (W.R. Turrell), ozhigin@pinro.ru (V. Ozhigin).
  [1] Tel.: +44 1224 876544; fax: +44 1224 295511.
  [2] Tel.: +7 8152 47 32 80; fax: +7 8152 47 33 31.
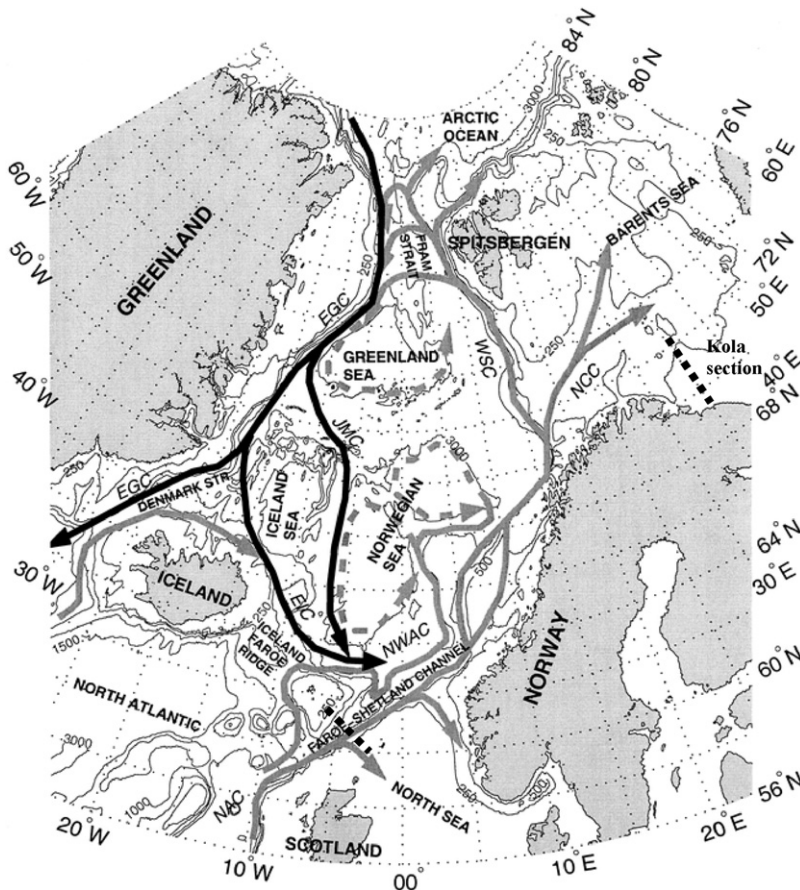
Fig. 1. Currents in the Nordic Seas: NAC—North Atlantic Current; NWAC—Norwegian Atlantic Current; NCC—North Cape Current; WSC—West Spitsbergen Current; EGG—East Greenland Current; EIC—East Icelandic Current; and JMC—Jan Mayen Current.

examined in this study, which presents for the first time comparisons between the annual mean sea level, temperature and salinity of Atlantic Water in the Faroe-Shetland Channel and the Kola section of the Barents Sea.

1.1. The Faroe-Shetland Channel

The Faroe-Shetland Channel is the deep-water channel separating the Faroese plateau from the Scottish continental shelf. The northern entrance from the Norwegian Sea is approximately 1500–2000 m deep. Connections to the Atlantic lie to the southwest through the Faroe Bank channel, with maximum depths of 850 m, and across the Wyville-Thomson Ridge, with a sill depth of approximately 450 m. Two standard hydrographic sections across the Channel have been surveyed by the Fisheries Research Services Marine Laboratory since the start of the 20th century. These lines run approximately from Fair Isle to Munken (Faroe) and from Nolso (Faroe) to Muckle Flugga (Shetland). They were first surveyed by Dr. H.N. Dickson, contracted to the Fishery Board for Scotland, onboard the fishery protection vessel HMS Jackal. He performed the first hydrographic station of the Nolso-Flugga section

on August 4, 1893. He went on to perform water bottle casts at four stations of the present day Nolso-Flugga section and at three stations of the Fair Isle-Munken section. Dickson resurveyed the same sections in 1896. Although fewer stations were performed during that survey, deeper casts were achieved, reaching >1000 m. Regular sampling at the full set of Nolso-Flugga and Fair Isle-Munken stations commenced in 1903 and has been performed approximately three times each year since that time, except for the war years and a 5-year period in the early 1980s.

A database of all available data collected along the two standard sections was constructed using data that existed in digital form from 1960 onwards and data from original manuscripts prior to that date. After the data was extracted, it was interpolated onto standard pressure levels. These procedures are more fully described in Turrell et al. (1999). In addition to data collected by the FRS Marine Laboratory, data from other sources—including Faroese, Norwegian, Swedish, Danish, English and Russian institutes—were obtained from ICES and entered into the database. Time-series derived from observations along the two sections have been employed in numerous previous publications (see Turrell et al., 1999).

In previous studies, time-series were constructed subjectively using manual methods from section plots and θ–S diagrams. Since the creation of the database, objective semi-automatic generation of time-series has been used in order to determine the characteristics of the different water masses observed along the sections. Two principal "types" of surface Atlantic water are always observed across the sections: a warmer and more saline type referred to as North Atlantic Water (NAW) and a fresher, cooler type referred to as Modified North Atlantic Water (MNAW). North Atlantic Water lies in the Slope Current, which flows northwards along the European shelf edge. Modified North Atlantic Water arrives at the standard sections after circulating around to the north of Faroe.

1.2. The Kola section

The Murman Fishery Research Expedition led by N. Knipovich occupied the Kola section for the first time in 1900 and was completed in 1906. During that period, the section was occupied one to six times per year. Subsequently, it was not occupied until 1921. In the 1920s and 1930s, the section was occupied from 1 (1924) to 10 (1937) times per year. The next gap in observations was during World War II. The section has been occupied more frequently since the middle of the 1950s, often with more than 12 surveys each year. In the 1970s and 1980s, the yearly number of occupations exceeded 15. A considerable decrease in occupation of the section occurred in the early 1990s. At that time and at present, PINRO took measurements along the section about 10 times per year. To date, the Kola section has been surveyed more than 950 times. The time-series of salinity began in 1951, owing to some uncertainties in the quality of the data collected during the first half of the 20th century. Quarterly and yearly temperature values from 1900 to 1920 and monthly temperature values from 1941 to 1981 were published by Bochkov (1982). Tereshchenko (1997) published monthly and yearly temperature and salinity values from 1951 to 1995.

The Kola section temperature time-series (Sts. 3–7, 0–200 m) can be used to assess seasonal and interannual variability of hydrographic conditions in the southern Barents Sea. There is a significant correlation ($R = 0.7$–0.9) between this time-series and those for stations 1–3 and 8–10 of the Kola transect (Tereshchenko, 1997). There is also a significant correlation ($R = 0.7$–0.9) between temperature time-series from the Kola section and other standard sections in the southern Barents Sea (North Cape-Bear Island section at the Barents Sea opening; Bear Island-East section (along 74°30′N) in the western Barents Sea; Cape Kanin-North section (along 43°15′E) in the eastern Barents Sea).

The Kola section time-series can serve as a reliable indicator of climate variability in the whole southern Barents Sea (coastal and Atlantic water domain). In addition, there is a significant correlation ($R = -0.56$ monthly data; $R = -0.65$ yearly data) between the time-series of temperature in the Kola section and ice coverage (percent of the total Barents Sea area). However, this is not true for the salinity time-series from stations 3 to 7, as correlation between temperature and salinity time-series from stations 3 to 7 is close to 0. This is probably due to the fact that there is a well-pronounced haline frontal zone (between 71°N and 72°N, Sts. 4–6) separating Atlantic water (warm temperature, high salinity) to the north and slightly warmer, considerably fresher coastal water to the south. Therefore, variability of salinity averaged for stations 3–7 may greatly depend on variations of the haline front position, but this is yet to be studied.

Stations 3–7 are usually associated with the Murman Current, which is the continuation of the North Cape Current entering the Barents Sea through its western boundary. The Murman Current is related to the haline/density frontal zone. According to calculations by a numerical model (Trofimov, 2000), the core of the current in the section is located at about 72°00′N.

The Kola section temperature and salinity time-series are often used in fisheries research and regional climate variability studies. Some examples can be found in the papers by Izhevskii (1961, 1964), Loeng (1989), Loeng et al. (1995), Ottersen et al. (1994, 2000), Yndestad (1999, 2003, 2006).

1.3. Regional climate indicators

The North Atlantic Water temperature and the Kola section water temperature represent long-term regional climate indicators. Better understanding of the causes of fluctuations of these indicators may lead to a better understanding of climate variability and forecast climate change. In this analysis, the variability in the climate indicators was characterised by the time-series spectrum properties. This spectrum may have information about the source of the deterministic properties that cause water mass characteristic fluctuations, including temperature. If these time-series have temporary deterministic properties, there is a possibility of forecasting dynamic change in the North Atlantic Water temperature, the Barents Sea water temperature and regional climate.

The present study compares the time-series of North Atlantic Water properties from the Faroe-Shetland Channel and the Kola section time-series. The cross-correlation between time-series of NAW temperature and Kola section temperature was estimated to be $R = 0.05$. This small correlation showed that the time-series fluctuations had different amplitude and phase.

In this study, the time-series was analyzed using a wavelet transform. This method made it possible to identify the amplitude and phase of dominant periodic cycles in each of the time-series and between time-series. The wavelet analysis showed that single dominant fluctuations were correlated to the lunar nodal tidal cycles of 18.6 and 9.3 years. The lunar nodal tide cycles have an astronomical property that made it possible to introduce a deterministic periodic reference in the cycle analysis, which added new information about the time-series properties.

2. Materials and methods

2.1. Faroe-Shetland Channel time-series

It has been shown that the best definition of the properties of North Atlantic Water, found within the core of the Slope Current on the Scottish side of the Faroe-Shetland Channel, is the temperature and salinity at the standard depth, which exhibits the maximum salinity within an individual survey of the first two stations in both standard sections on the Scottish side of the Channel. As the standard section surveys in the past were performed at quite different times of year in order to remove the effect of the seasonal cycle in the surface waters and, hence, to allow all data to be used, the monthly mean temperature and salinity derived over the period from 1960 to 1995 for each individual station and at each standard depth were removed prior to smoothing the data using a 2-year centered running mean. Therefore, the data are expressed as anomalies. The time-series covers 1893, …, 2002 and has missing values for 1895, …, 1902, 1915, …, 1922, 1930, …, 1933, 1941, …, 1946. In these periods, the data were cubic interpolated.

For Modified North Atlantic Water, located on the Faroese side of the channel, the definition used was the temperature and salinity at the standard depth, which exhibited the maximum salinity within an individual survey of the first two stations in both standard sections on the Faroese side of the Channel. Again, the seasonal cycle was removed prior to smoothing using a 2-year running mean. Therefore, the data are presented as anomalies. The time-series covers 1893, …, 2002 and has missing values for 1895, …, 1902, 1915, …, 1922, 1930, …, 1933, 1941, …, 1946. In these periods, the data were cubic interpolated.

2.2. Barents Sea time-series

The data used here were monthly temperature values from the upper 200 m in the Kola section along the 33°30′E medial from 70°30′N to 72°30′N in the Barents Sea (Bochkov, 1982; Tereshchenko, 1997). The temperature time-series contained quarterly and annual values from the period 1900 to 2005 and monthly values from 1921 to 2005, some of which were measured and some of which were calculated. The gaps in the time-series were filled by Bochkov (1982) by means of calculations by multiple regression models. To calculate quarterly and yearly temperatures for 1900–1920 and 1941–1944, air temperature at stations Kola and Polyarny, ice coverage of the Barents Sea (percent of the total area), number of deep low pressure cells (cyclones) over the Nordic Seas and a ratio of the number of deep cyclones over the Barents Sea to the number of deep cyclones over the Nordic Seas were all used as the independent variables in the regression models. The models were fitted to the data from 1946 to 1974. Their quality was evaluated by means of comparison to temperature calculated by models and that observed in 1921–1940. Coefficients of correlation between calculated and observed temperatures ranged from 0.88 to 0.93.

Standard deviations of differences between calculated and observed values, i.e. standard errors, were less than probable errors. Owing to high correlation between monthly and quarterly time-series, monthly temperature values for 1941–1944 were calculated by simple regression models, and quarterly temperature time-series were used as independent variables. Thus, quarterly and yearly temperature values are available from 1900 to 2005, and the monthly time-series begins in 1921. Salinity time-series (monthly and annual values) is available only from the period 1951 to 2004. This paper analyzes the annual mean temperature and salinity.

2.3. Sea-level time-series

The time-series of sea level at Aberdeen and Murmansk were provided by the Proudman Oceanographic Laboratory, UK. These time-series had an annual mean and covered the period 1931 to 2002. The Stockholm sea level time-series is published by Ekman (1999, 2003) and covers the period from 1774 to 2003. The time-series was detrended before the wavelet analysis.

2.4. The time-series spectrum

The present analysis is based on the hypothesis that the astronomic 18.6-year lunar nodal cycle introduces a set of harmonic and sub-harmonic gravity cycles, which in turn introduces a lunar nodal tide spectrum. The lunar nodal tide spectrum may be represented by the model:

$$x(t) = u(t) + v(t)$$
$$u(t) = \sum_k a_k(t) \sin(k\omega_T t + \varphi_{kT}(t)), \tag{1}$$

where $x(t)$ represents a measured time-series; $u(t)$ is the lunar nodal harmonic cycles; $v(t)$ is a disturbance from an unknown source; $a_k(t)$ is the cycle amplitude; $\omega_T = 2\pi/T$ (rad year^{-1}), the cycle period; and $\varphi_{kT}(t)$, the time-dependent phase angle. Cycle number k may have values $k = 1, 2, 3, …$ on harmonic cycles, $k = 1/2, 1/3, …$ on sub-harmonic cycles in the lunar nodal spectrum and the time $t = 1900, 1901, …, 2005$.

The astronomic lunar nodal amplitude cycle of $T = 18.6134$ years introduces a periodic tide that has vertical and horizontal components. The vertical component has a global influence on the sea level and has maximum influence at the Equator and the Arctic Ocean and a minimum at about 30° from the Equator. The horizontal component influences the tidal current, which has a maximum at about 30° from the Equator. This nodal amplitude tide had a maximum in November 1987, which represented a phase delay of about $\varphi_T(t) = 0.90\pi$ (rad) in Eq. (1). The vertical amplitude tide caused a current component that had a phase angle of about $\varphi_T(t) = (0.90–0.50)\pi$ (rad). The resulting current phase was dependent on latitude and current conditions. The amplitude tide introduced a lunar nodal phase tide, which had a period time of $T/2 = 9.3$ years and a phase angle of about $\varphi_{T/2}(t) = 1.41\pi$ (rad) (Pugh, 1996; Boon, 2004). This investigation identified a sub-harmonic cycle of about

$4 \times 18.6 = 74.4$ years by the estimated phase angle $\phi_{4T}(t) = 0.55\pi$ (rad), which served as a reference in the analysis.

2.5. Time-series spectrum identification

Traditional methods of spectrum analysis cannot identify cycle periods and cycle phase in time-variant stochastic processes. In this study, therefore, the time-series were analyzed by wavelet transformation in order to identify the dominant cycle periods $u_{kT}(t)$ and the time-variant phase angle $\varphi_{kT}(t)$. The periodicity was identified by a three-step investigation. The first step was to compute the wavelet spectrum by the transformation:

$$W_{a,b}(t) = \frac{1}{\sqrt{a}} \int_R x(t) \Psi\left(\frac{t-b}{a}\right) dt, \tag{3}$$

where $x(t)$ is the time-series analyzed and $\Psi(\ )$ is a coiflet wavelet impulse function (Daubechies, 1992; Matlab, 1997). $W_{a,b}(t)$ is a set of wavelet cycles; b is the translation in time; and a is the time-scaling parameter in wavelet transformation. The relationship between the wavelet scaling a and a sinus period T was about $T \approx 1.2a$. In this analysis, the translation $b = 0$, so the computed wavelet transformation $W_a(t)$ represented a moving correlation between $x(t)$ and the impulse function $\Psi(\ )$ over the whole time-series $x(t)$.

Using this wavelet transformation, it was possible to identify single, long-period cycles in short time-series. Errors at the beginning and end of a time-series were reduced in the following manner. The time-series were scaled in amplitude and to zero mean value by the scaling transformation $y(t) = [x(t)-\text{mean}(x(t))]/\text{var}(x(t))$, where $x(t)$ is the time-series, and $y(t)$ is the scaled time-series. Subsequently, the time-series was expanded with symmetrical values at the beginning and end of the time-series (the 'sym' parameter in Matlab).

Time-series $x(t)$ may be represented by summing the dominant wavelets that contain most of the energy in time-series $x(t)$. The time-series may then be represented by

$$x(t) = \sum_k W_{ak}(t) + v(t) = W(t) + v(t), \tag{4}$$

where $W(t)$ represents all the dominant wavelet cycles and $v(t)$ is disturbance from an unknown source. A wavelet cycle represents a moving correlation between the time-series and a wavelet impulse $\Psi(\ )$ scaled by a. A single, dominant-wavelet cycle $W_{ak}(t)$ thus represents the best correlation with scale a. The dominant-wavelet cycles $W(t)$ have dominant amplitude in the wavelet spectrum.

The cycle periods of single dominant-wavelet cycles are identified by computing the autocorrelation for the wavelet spectrum $R_w(\tau) = E[W_a(t)W_a(t)]$. Dominant, stationary wavelet cycles have maximum values in the autocorrelation functions. Periodic cycles in the autocorrelation function demonstrate there is a stationary cycle. The cycle period phase is identified by the optimum cross-correlation between dominant wavelets and lunar nodal

cycles by $R_{kT}(\tau) = E[W_{ak}(t)u_{kT}(t)]$, where $u_{kT}(t)$ is a kT lunar nodal cycle period, and the phase angle $\varphi_{kT}(t)$ is a free variable. Correlation quality is computed by the Pearson correlation coefficient:

$$Q_{kT} = R_{kT}\sqrt{\frac{n-2}{1-R_{kT}^2}} \sim t(n-2), \tag{5}$$

where n is the number of samples. Q_{kT} is tested against a t-distribution by $(n{-}2)$ degrees of freedom to see whether the correlation is statistically significant (Daly et al., 1995; von Storch and Zwiers, 1999).

3. Results

3.1. Aberdeen annual mean sea level

Fig. 2 shows the annual mean sea level $x(t)$ at Aberdeen, the dominant 18-year wavelet cycle $W_{18}(t)$ and the astronomic 18.6-year lunar nodal amplitude tide $u_T(t)$. The long-term fluctuation of the annual sea level was analyzed from the wavelet spectrum $W_{1:N/2}(t)$ of the Aberdeen sea level time-series (Eq. (3)). This transform represented a moving linear filter that separated periodic cycles in the time-series. The fluctuation had maxima at about $t = \{1950, 1990\}$ and minima at about $t = \{1940, 1975\}$. The periodic cycle time was identified by taking an autocorrelation $R_w(\tau)$ of the wavelet spectrum $W_{1:N/2}(t)$. The autocorrelation $R_w(\tau)$ identified dominant wavelet cycles at $\tau = \{9, 18, 28, 39, \ldots\}$ years and $\tau = \{19, 38, 56\}$ years. This additive pattern indicated that the annual mean sea level had stationary dominant cycles of about 9 and 19 years in the time-series.

The dominant 18-year wavelet cycle $W_{18}(t)$ had an estimated phase angle $\varphi_T(t) = (0.90{-}0.1)\pi$ (rad), which was close to the astronomic vertical lunar nodal cycle period. The correlation between the 18-year wavelet cycle, $W_{18}(t)$, and the lunar nodal amplitude tide cycle $u_T(t)$ was $R_T = 0.88$, where the quality was $Q_T = 42$ and the number of samples was $N = 70$. The estimate showed that the dominant 18 year cycle, $W_{18}(t)$, was correlated with the 18.6-year astronomical lunar nodal amplitude tide cycle.

Fig. 3 shows the time-series of Aberdeen sea level, the astronomic 18.6-year amplitude tide $u_T(t)$ and the lunar nodal phase tide cycle $u_{T/2}(t)$. The figure demonstrates well the close relationship between the sea level fluctuations, the 18.6-year astronomical amplitude cycle $u_T(t)$ and the 9.3-year phase cycle $u_{T/2}(t)$. The Aberdeen sea level had minimum values at about $t = \{1940, 1978\}$, when the astronomic cycles had minimum values, and maximum values at about $t = \{1950, 1970, 1990\}$, when the astronomic cycles were positive. The correlation between the 9.3 year phase tide $u_{T/2}(t)$ and the dominant 9 year wavelet $W_9(t)$ was estimated at $R_{T/2} = 0.39$, with quality $Q_{T/2} = 3.1$ when $N = 70$. The phase angle was estimated at $\varphi_{T/2}(t) = (1.41{-}0.65)\pi$ (rad). Fig. 3 shows that the 9.3 year tide had a maximum when the 18.6 year tide had phase angles of $\varphi(t) = 3\pi/4$ and $7\pi/4$ (rad).
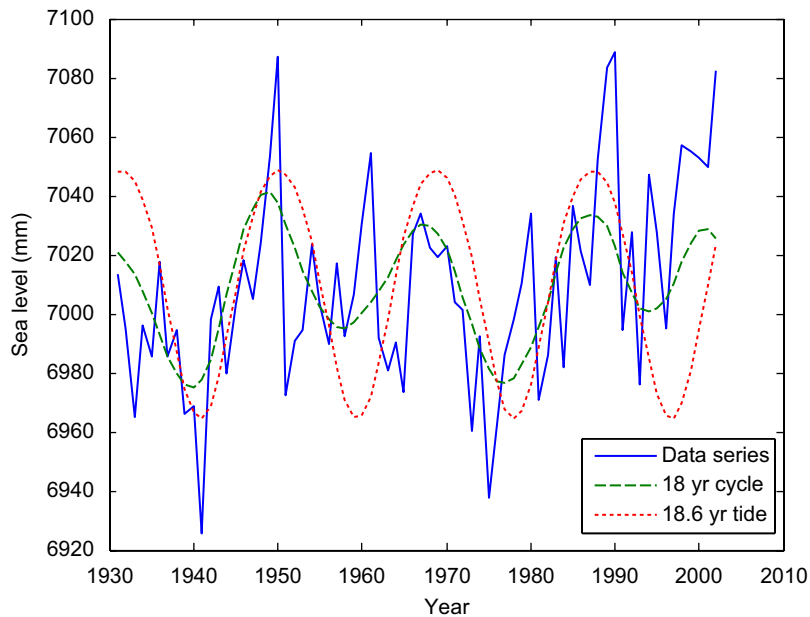
Fig. 2. The annual mean Aberdeen sea level (mm): the identified 18-year-dominant wavelet and the 18.6-year lunar nodal cycle.
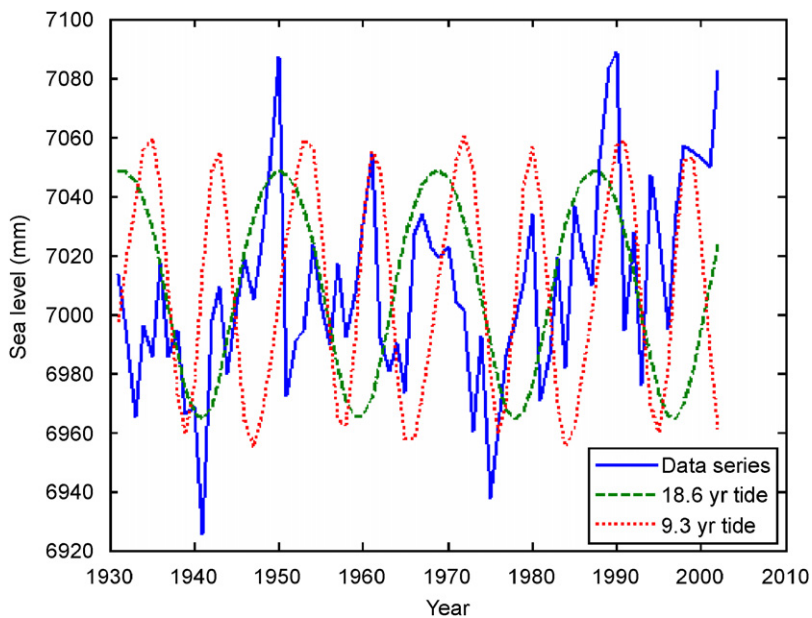
Fig. 3. Aberdeen annual mean sea level, the 18.6- and 9.3 years tide.

The wavelet analysis method demonstrates well the ability to identify cycle period and phase in the time-series. The wavelet identification of the 9.3-year phase tide explains the high fluctuations when the amplitude tide and the phase tide have the same phase. This tide is here identified for the first time in a North Atlantic time-series. Time-series from nature are expected to have a non-correlated spectrum. The identification of the amplitude tide and phase tide makes it possible to use stable astronomic periodic cycles as a reference for temperature and salinity fluctuations.

3.2. Stockholm annual mean sea level

The Aberdeen sea level time-series was too short to identify potential sub-harmonic periods from the 18.6-year tide. The monitored sea level time-series from 1774 to 2000 at Stockholm represents the longest sea level time-series in the world (Ekman, 1999, 2003). Fig. 4 shows a detrended representation of the Stockholm time-series, the dominant 74-year cycle from the wavelet spectrum and the $4 \times 18.6 = 74.4$ year sub-harmonic cycle. Wavelet
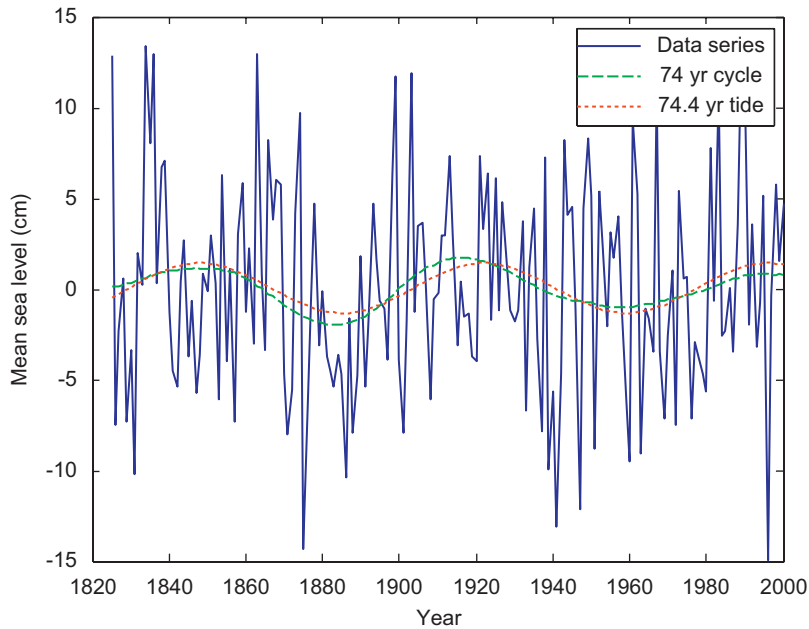
Fig. 4. Detrended annual mean sea level anomaly fluctuation at Stockholm from 1825 to 2000, dominant 74-year cycle and 74.4-year sub-harmonic tide.

analysis of this time-series identified the same lunar nodal spectrum as in the Aberdeen sea level time-series. The Stockholm sea level time-series had a correlation $R_T = 0.5$ and a quality $Q_T = 8.2$ to the 18.6-year lunar nodal cycle at the phase angle $\varphi_T(t) = (0.90+0.5)\pi$ (rad). The long-term fluctuation had a correlation $R_{4T} = 0.93$ and a quality $Q_{4T} = 32$ from 1825 to 2000 to the sub-harmonic cycle of $4 \times 18.6 = 74.4$ years at the phase angle $\varphi_{4T}(t) = 0.55\pi$ (rad) (Fig. 4).

Wavelet analysis of the Stockholm time-series showed that the sea level had long-term fluctuations related to sub-harmonics of the forced 18.6-year lunar nodal tide. Closer investigation showed the 18-year cycle had a small phase-disturbance in the period from 1850 to 1925, when the 74-year cycle had a maximum. This disturbance reduced the correlation to the lunar nodal spectrum. The 74-year harmonic cycle is most likely being identified for the first time in long sea level time-series.

3.3. North Atlantic water temperature

Fig. 5 shows the time-series of North Atlantic Water (NAW) temperature anomaly (i.e. seasonal; cycle removed) on the Scottish side of the Faroe-Shetland Channel from 1900 to 2005. The time-series demonstrates that the temperature had large fluctuations over a period of 100 years. The data showed some extreme values in the cubic interpolated portions in about 1920 and 1945. The temperature anomaly fluctuates from about $-1.4\,°C$ in 1920 to about $0.9\,°C$, and in 1945 and 1967, the temperature anomaly decreased to about $-0.5\,°C$. The wavelet amplitude spectrum $W_a(t)$ (Fig. 6) showed that the time-series had some dominant cycle periods. An autocorrelation of the wavelet spectrum, $W_a(t)$, showed

the wavelet spectrum had dominant periods of about $\tau = \{9, 18, 27, 36, 55, 75\}$ years and indicated a strong harmonic cycle of about 9 years. The long-term cycle had maxima in about 1945 and 2005 and minima in about 1915 and 1975, which was close to the sea level long-term trend.

Fig. 5 shows the relationship between the NAW temperature anomaly $x(t)$, the 74-year harmonic lunar nodal cycle $u_{4T}(t)$, the 18-year wavelet cycle $W_{18}(t)$ and the astronomic 18.6-year lunar nodal tide $u_T(t)$. The identified 18-year wavelet cycle $W_{18}(t)$ had an estimated phase of about $\varphi_{18}(t) = (0.90-0.00)\pi$ (rad) in the period from 1900 to about 1925. In the period from 1925 to 2004, the 18-year wavelet cycle phase shifted to about $\varphi_{18}(t) = (0.90-0.85)\pi$ (rad), which represented a phase reversal. In this period, the correlation with the astronomic 18.6-year lunar tide was estimated at $R_T = -0.68$, $Q_T = 8.3$ and $N = 80$.

The identified 74-year wavelet cycle, $W_{74}(t)$, had a phase of about $\varphi_{4T}(t) = (0.55-0.36)\pi$ (rad) and a correlation of $R_{4T} = 0.93$, $Q_T = 27.8$ and $N = 104$ with the sub harmonic cycle $u_{4T}(t)$. This means there is an estimated phase delay of about 0.36π (rad) between the 74-year tidal cycle and the 74-year cycle of NAW temperature. Figs. 4 and 5 show that the 74-year temperature cycle had a turning point at about 1960, when the 74-year tidal cycle turned in a positive direction. In this short time-series, the 74-year cycle period represents a moving average of the temperature fluctuations in NAW.

Fig. 7 shows the NAW temperature anomaly time-series $x(t)$, the estimated dominant 9-year wavelet cycle $W_9(t)$ and the astronomic phase cycle $u_{T/2}(t) = 18.6/2 = 9.3$-year lunar nodal tide. The astronomic 9.3-year tide $u_{T/2}(t)$ had a cycle phase of $\varphi_{T/2}(t) = 1.41\pi$ (rad)
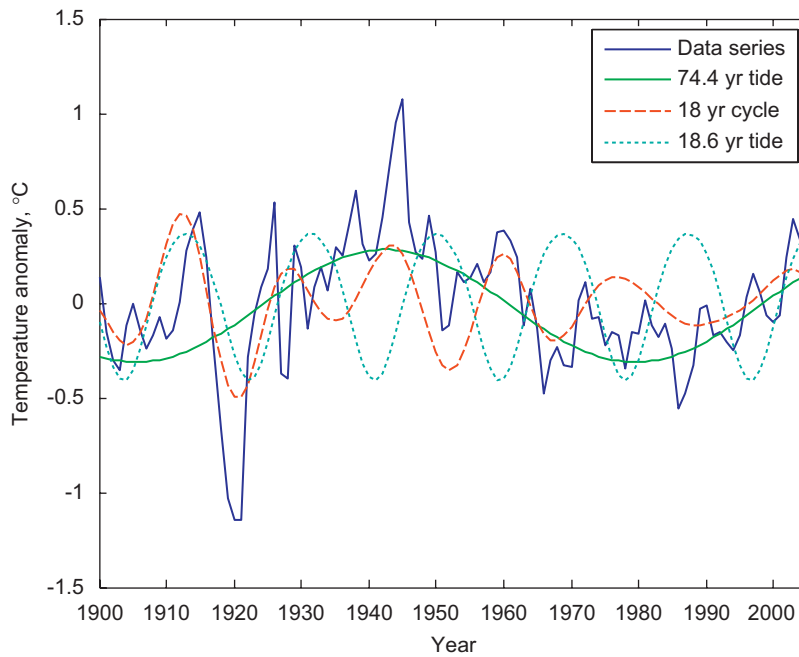
Fig. 5. NAW temperature anomaly (i.e. seasonal cycle removed) $x(t)$, 74-year harmonic lunar nodal cycle $u_{4T}(t)$, the 18-year wavelet cycle $W_{18}(t)$ and the astronomic 18.6-year lunar nodal tide $u_T(t)$.
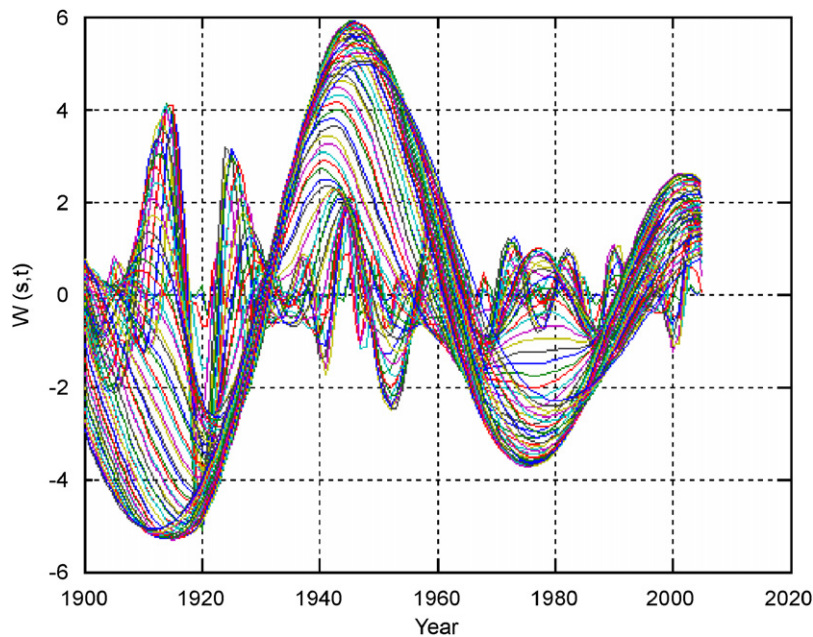
Fig. 6. The NAW wavelet spectrum $W_a(t)$.

and was associated with maximum changes in the 18.6-year lunar nodal cycle in the positive or negative direction. The 9-year wavelet cycle $W_9(t)$ and the astronomic cycle $u_{T/2}(t)$ had the same phase in the periods 1900 to 1922 and from about 1960 to 2000, when the 74-year sub-harmonic cycle $u_{4T}(t)$ was in a negative state.

When $u_{4T}(t)$ was in a positive state from about 1922 to 1960, the wavelet cycle phase was identified to be about $\varphi_{T/2}(t) = (1.41-0.65)\pi$ (rad). The correlation with a stationary cycle was estimated at $R_{T/2} = 0.59$, $Q_{T/2} = 4.7$ and $N = 42$ from 1960 to 2002. This analysis showed that the astronomic 9.3-year phase tide influenced temperature
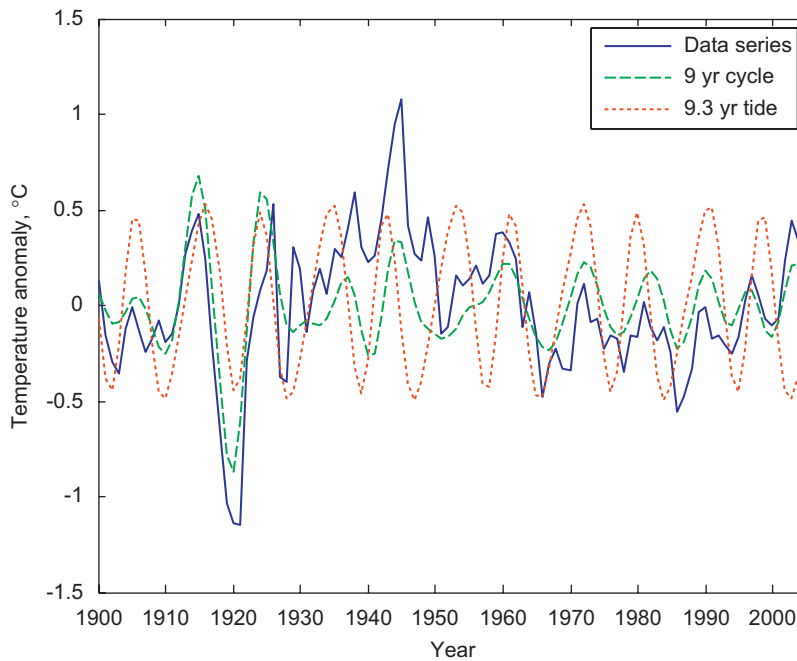
Fig. 7. The NAW temperature anomaly (i.e. seasonal cycle removed) data series $x(t)$, the 9-year wavelet cycle $W_9(t)$ and the astronomic 9.3-year lunar nodal tide $u_{T/2}(t)$.

fluctuations in North Atlantic Water. This fluctuation had a stable period and a temporary stable phase.

The wavelet spectrum analysis of NAW showed that the dominant temperature fluctuations were correlated with the lunar nodal period cycles of 9.3, 18.6 and 74.4 years. The 9.3-year phase had an estimated phase angle of about 0.65π (rad). This phase angle suggests that Atlantic Water properties are established before water masses arrive at the Faroe-Shetland Channel.

3.4. North Atlantic water salinity

Fig. 8 shows the time-series of the NAW salinity anomaly (i.e. seasonal cycle removed) on the Scottish side of the Faroe-Shetland Channel from 1900 to 2005. The salinity increased from a minimum in 1910 to a maximum around 1940, when the sea level was at a minimum. From 1940, the salinity decreased to a new minimum around 1975, but the salinity continues to increase today.

The wavelet amplitude spectrum $W_{1:N/2}(t)$ had some strong periodic fluctuations in the period from 1900 to 2005. The long-term fluctuation had a maximum in about 1945 and minima at about $t = \{1910, 1980\}$. The auto-correlation wavelet spectrum $R_w(\tau)$ had dominant wavelet cycle periods of about $\tau = \{9, 18, 27\}$, $\tau = \{14, 30, 63\}$ and $\tau = \{33, 63\}$ years. This indicated a more complex spectrum in the time-series.

The NAW salinity anomaly time-series had dominant cycles of about 74, 18 and 9 years. The 74-year wavelet, $W_{74}(t)$, had an estimated phase angle $\varphi_{4T}(t) = (0.55–0.26)\pi$ (rad). The correlation to a 74.4-year sub-harmonic cycle $u_{4T}(t)$ was estimated at $R_{4T} = 0.99$,

$Q_{4T} = 86$ when $N = 101$. The 18-year wavelet cycle $W_{18}(t)$ had phase reversals related to the polarity of the 74-year wavelet cycle.

The phase of the dominant 18-year wavelet cycle $W_{18}(t)$ was estimated at $\varphi_T(t) = (0.90–0.25)\pi$ (rad) when $u_{4T}(t)$ was in a negative period from 1900 to 1925; $\varphi_T(t) = (0.90–1.00)\pi$ (rad), in the period from 1925 to 1960 when $u_{4T}(t)$ was in a positive state; and $\varphi_T(t) = (0.9–0.0)\pi$ (rad), in the period from 1960 to 2000 when $u_{4T}(t)$ was in a negative state (Fig. 5). The phase-reversal indicated an interference between the 18 and the 74 years cycles, $W_{18}(t)$ and $W_{74}(t)$.

Fig. 9 shows the NAW salinity anomaly (i.e. seasonal cycle removed) $x(t)$, 18.6-year lunar nodal cycle $u_T(t)$ and the 9-year wavelet cycle $W_9(t)$. In this analysis, the dominant 9-year wavelet cycle $W_9(t)$ had an estimated phase of $\varphi_{T/2}(t) = (1.41–0.31)\pi$ (rad) and a correlation of $R_{T/2} = 0.41$, $Q_{T/2} = 45$ and $N = 101$. This analysis indicated that the astronomic 9.3-year phase tide introduced a stable fluctuation in the whole time-series. The salinity anomaly had a maximum in 1941, when the 74, 18 and 9 years cycle also had maxima.

The wavelet spectrum analysis of the NAW salinity anomaly time-series showed that the dominant fluctuations were correlated to the 9.3-year phase tide, the 18.6-year amplitude tide and the 74.4-year sub-harmonic cycle. The NAW temperature had a phase-reversal related to the mean 74-year fluctuation. The NAW salinity had a more complex phase relation, the cause of which was unclear. It may be described by the model $u_m(t) = -\sin(\omega_T t + (0.9–0.1)\pi) \times \sin(\omega_T t/4 + (0.55–0.26)\pi)$. The correlation between $W_{18}(t)$ wavelet and the modulated cycles $u_m(t)$ was estimated at $R_m = 0.82$, $Q = 12.3$ and $N = 75$.
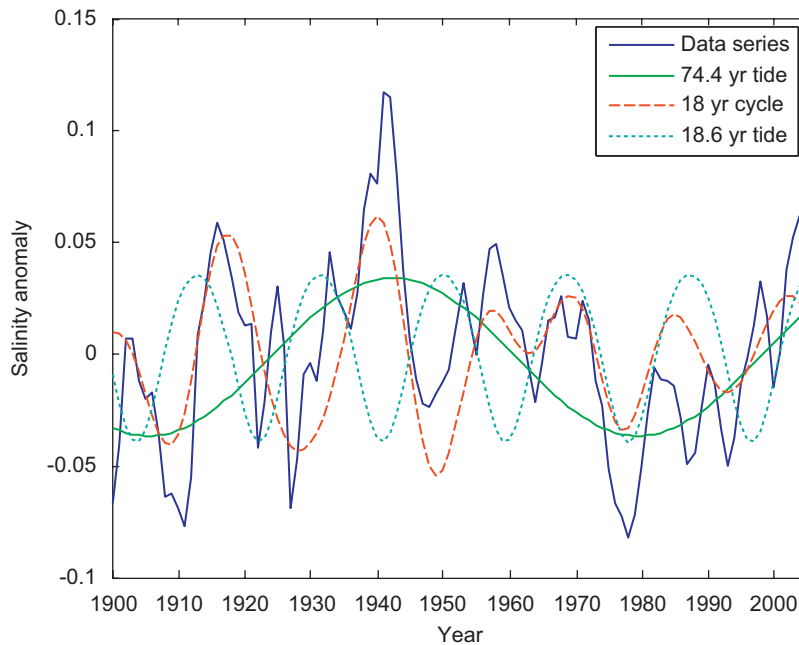
Fig. 8. The NAW salinity anomaly (i.e. seasonal cycle removed) $x(t)$, 74-year harmonic lunar nodal cycle $u_{4T}(t)$, the 18-year wavelet cycle $W_{18}(t)$ and the astronomic 18.6-year lunar nodal tide $u_T(t)$.
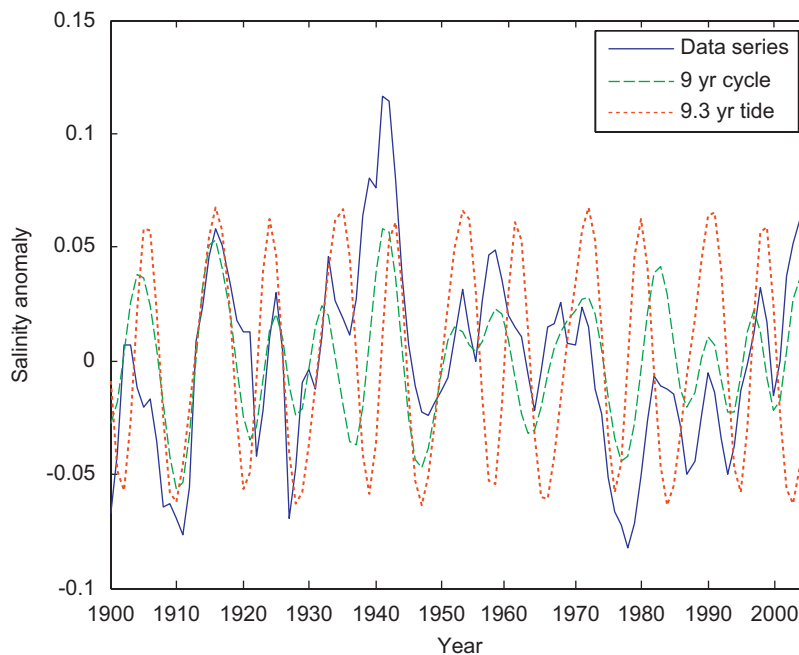
Fig. 9. The NAW salinity anomaly (i.e. seasonal cycle removed) $x(t)$, 18-year harmonic lunar nodal cycle $u_T(t)$ and the 9-year wavelet cycle $W_9(t)$.

3.5. Modified North Atlantic water temperature

Modified North Atlantic water (MNAW) flows northwards west of the Rockall Plateau and crosses the Iceland-Faroe ridge to flow north of Faroe before it enters the Faroe-Shetland Channel from the east. Fig. 10 shows the MNAW temperature anomaly (i.e. seasonal cycle

removed) time-series $x(t)$, 74-year harmonic lunar nodal cycle $u_{4T}(t)$, the 18-year wavelet cycle $W_{18}(t)$ and the astronomic 18.6-year lunar nodal tide $u_T(t)$. The dominant periodic cycles found for MNAW salinity had properties similar to those estimated for the NAW time-series. The identified 74-year wavelet cycle $W_{74}(t)$ had a phase angle of about $\varphi_{4T}(t) = (0.29{-}0.05)\pi$ (rad) and a correlation of
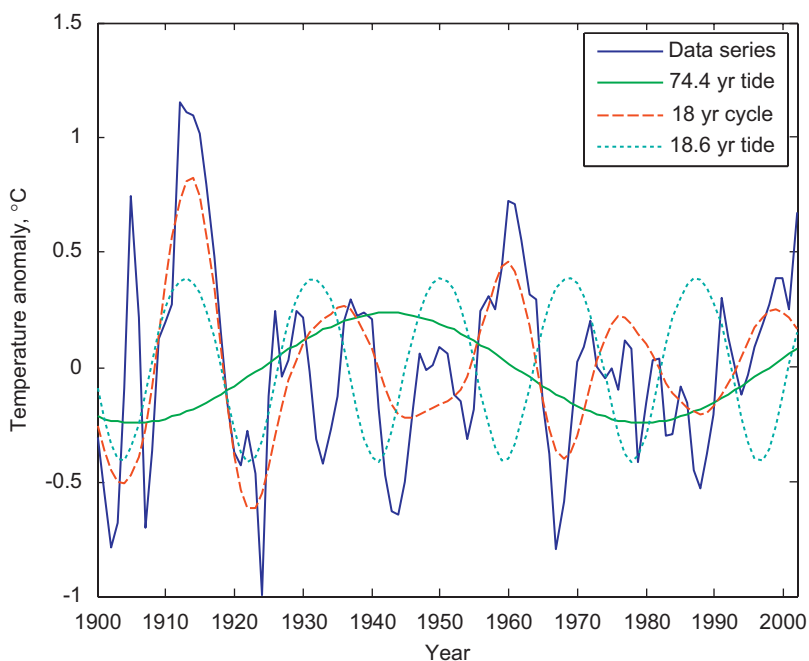
Fig. 10. MNAW temperature anomaly (i.e. seasonal cycle removed) $x(t)$, the 74-year harmonic lunar nodal cycle $u_{4T}(t)$, the 18-year wavelet cycle $W_{18}(t)$ and the astronomic 18.6-year lunar nodal tide $u_T(t)$.
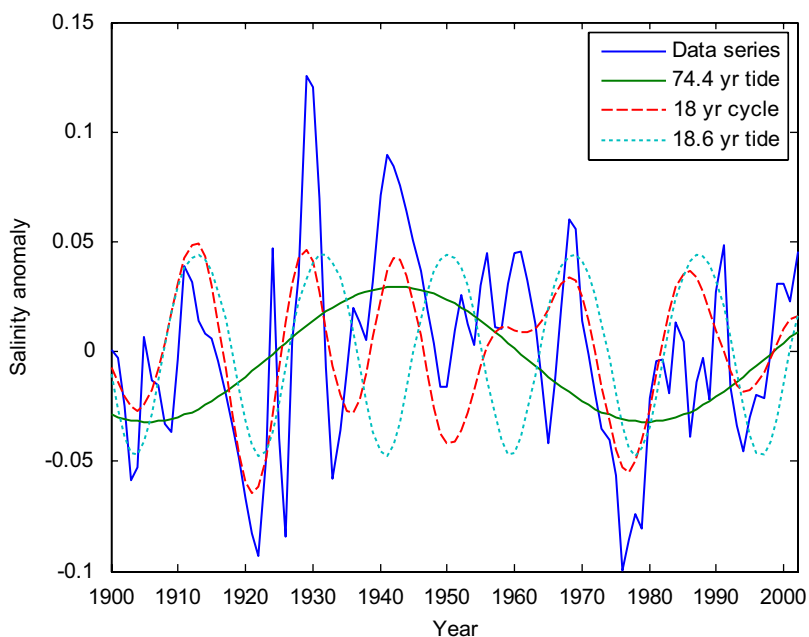
Fig. 11. The MNAW salinity anomaly (i.e. seasonal cycle removed) $x(t)$, the 74-year harmonic lunar nodal cycle $u_{4T}(t)$, the 18-year wavelet cycle $W_{18}(t)$ and the astronomic 18.6-year lunar nodal tide $u_T(t)$.

$R_{4T} = 0.82$, $Q_T = 14.7$ and $N = 104$ to the sub-harmonic cycle $u_{4T}(t)$. The dominant 18-year cycle had a phase-reversal to about $\varphi_T(t) = (0.90–0.90)\pi$ (rad) from about 1925, when the 74-year cycle moved from a negative to a positive state. In the period from 1925 to 2000, the correlation was estimated to be about $R_T = 0.69$, $Q_T = 8.0$ when $N = 70$ from 1930.

Fig. 11 shows the MNAW salinity anomaly time-series $x(t)$, 74-year harmonic lunar nodal cycle $u_{4T}(t)$, the 18-year wavelet cycle $W_{18}(t)$ and the astronomic 18.6-year lunar

nodal tide $u_T(t)$. In this case, the 74-year cycle had an estimated phase angle $\varphi_{4T}(t) = (0.29-0.10)\pi$ (rad) and a correlation of $R_{4T}(t) = 0.82$, $Q_{4T} = 17.7$, when $N = 108$.

The time-series of NAW and MNAW had the same dominant periods correlated to the lunar nodal cycles of 9.3, 18.6 and 74.4 years. The dominant 18-year cycle in MNAW salinity had a complex fluctuation that may be represented by the multiplicative modulation model $u_m(t) = -\sin(\omega_T t + (0.9-01)\pi) \times \sin(\omega_T t/4 + (0.55-0.26)\pi)$. The correlation between the model and the 18-year cycle was estimated at $R_m = 0.5$, $Q_m = 5.7$ in the total time-series of $N = 108$ samples.

3.6. Murmansk annual mean sea level

Wavelet analysis identified the same dominant 18- and 9-year cycles as found for the Aberdeen time-series. In this case, the optimum correlation between $W_{18}(t)$ and $u_T(t)$ was estimated at $R_T = 0.70$, $Q_T(t) = 7.0$ and $N = 50$ at the phase angle $\varphi_T(t) = (0.90-0.20)\pi$. The 9.3-year phase tide had an estimated correlation $R_{T/2} = 0.80$ and $Q_{T/2} = 9.3$ at the phase angle at $\varphi_{T/2}(t) = (1.41-0.90)\pi$ (rad).

The Murmansk time-series had the same dominant 18.6-year amplitude tide and 9.3-year phase tide cycles as identified in the annual mean sea level at Aberdeen. The difference was a time delay of about a year on the amplitude tide and about 2 years on the phase tide.

3.7. Kola section temperature

The Kola section temperature time-series covers the time period from 1900 to 2005 (Fig. 12). The data indicates that there was a warming trend from about 1900 to 1940,

followed by cooling until about 1980 and, after that, continued warming. The Kola section temperature wavelet spectrum $W_{1:N/2}(t)$ had short and long-term fluctuations. The long-term fluctuation had a maximum in about 1945 and minima at about $t = \{1910, 1975\}$. This was the same fluctuation period as in North Atlantic Water. The autocorrelation $R_w(\tau)$ of the wavelet spectrum $W_a(t)$ showed periodic cycles of about $\tau = \{9, 18, \ldots\}$ years and $\tau = \{18, 32, \ldots\}$ years. This indicated that we could expect periodic cycles of about 9 and 18 years in the Kola section temperature time-series.

Fig. 12 shows the Kola section temperature $x(t)$, the stationary 74-year cycle $u_{4T}(t)$, identified 18-year cycle $W_{18}(t)$, and the 18.6-year lunar nodal cycle $u_T(t)$. In this short time-series, long-term cycles of about 74 years were identified in the wavelet spectrum $W_a(t)$. The 74-year cycle had a cycle phase of about $\varphi_{4T}(t) = (0.55+0.71)\pi$ (rad), which was about the same phase as the identified 74-year NAW temperature cycle. The correlation with the 74-year subharmonic cycle was estimated at $R_{4T} = 0.95$, $Q_{4T} = 32.6$ in the period from 1900 to 2004. Fig. 12 shows that the stationary cycle $u_{4T}(t)$ follows the running mean temperature fluctuation. This supports the hypothesis that the 74-year cycle represents a running mean temperature fluctuation.

The estimated 18-year wavelet cycle $W_{18}(t)$ had a phase angle $\varphi_T(t) = (0.90-1.30)\pi$ (rad) in the period from 1900 to 1920. In about 1920, the 18-year wavelet cycle had a phase-reversal to $\varphi_T(t) = (0.90-0.20)\pi$ (rad). The estimated correlation to the stationary lunar nodal cycle $u_T(t)$ was estimated at $R_T = 0.77$ and $Q_T(t) = 10.0$ in the period from 1920 to 2004. The 18-year cycle had a phase delay of about 0.2π (rad) in relation to the astronomic 18.6-year nodal cycle.

Fig. 13 shows the Kola section temperature time-series, the estimated 9-year wavelet cycle $W_9(t)$ and the 9.3-year
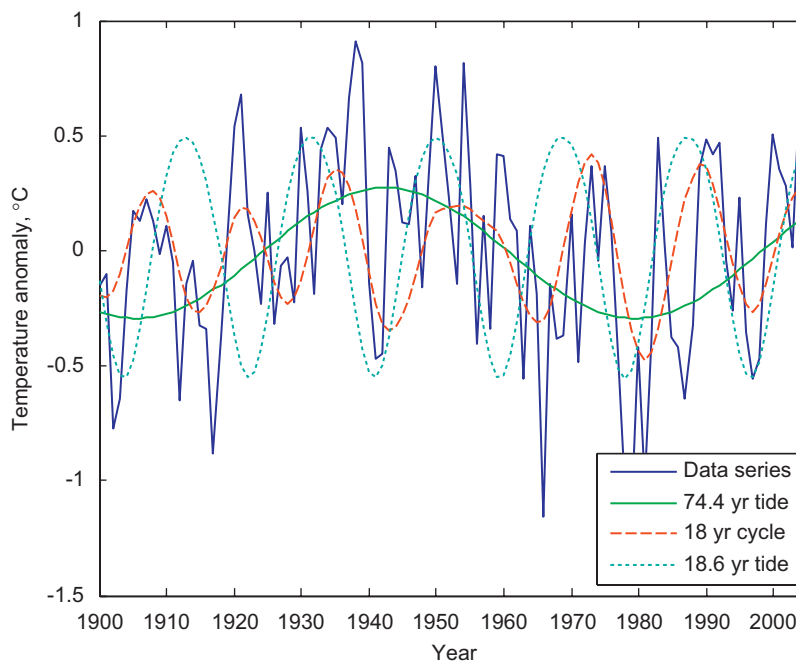
Fig. 12. The Kola section temperature anomaly, stationary 74-year cycles, identified 18-year cycle and 18.6-year lunar nodal cycle.
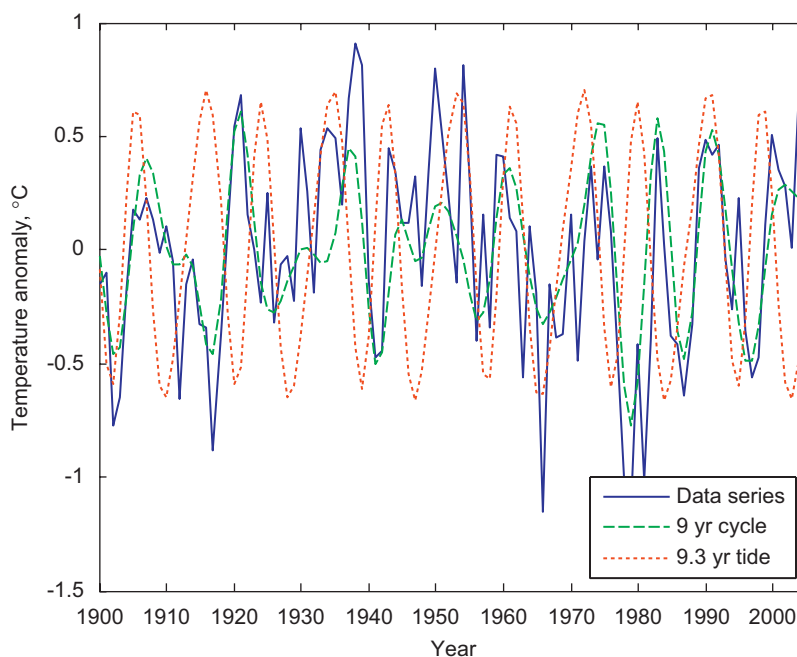
Fig. 13. Kola section temperature anomaly, identified 9-year wavelet and 9-year lunar nodal cycles.

lunar nodal phase cycle $u_{9.3}(t)$. In this time-series, the phase angle of the wavelet cycle $W_9(t)$ was estimated at $\varphi_{T/2}(t) = (1.41-1.00)\pi$ (rad). The correlation to the 9.3-year tide $u_{T/2}(t)$ was estimated at $R_{T/2} = 0.74$, with the correlation quality $Q_{T/2} = 6.9$ in the period from 1960 to 2005. The identified dominant 9-year cycle was related to the 9-year cycle in the Murmansk annual sea level. The cycle was stable in the period from 1960 to about 2005, when the 74-year cycle was in a negative state. In this period, the 9-year Kola temperature and 9-year phase tide had reversed phase.

3.8. Kola section salinity

The Kola section salinity time-series was measured from about 1950 to 2004 and salinity was estimated to be 34.82 in 2005. Fig. 14 shows that this time-series has large fluctuation in the period from 1950 to 1975. There was then a mean reduction of the salinity, which then continued to increase from about 2000. In this time-series, the autocorrelation $R_a(\tau)$ spectrum had periods of about 11 and 18 years.

Fig. 14 shows the Kola section salinity time-series $x(t)$, the estimated 18-year wavelet cycle $W_{18}(t)$ and the astronomical lunar nodal cycle $u_T(t)$. In this time-series, the dominant 18-year wavelet cycle had an estimated phase angle $\varphi_T(t) = (0.90-0.30)\pi$ (rad). The correlation between the 18-year wavelet cycle and the 18.6-year astronomical lunar nodal cycle was estimated at $R_T = 0.9$ and $Q_T = 9.4$. The 18-year salinity cycle was related to the 18-year temperature cycle and the 18-year sea level cycle.

Fig. 15 shows the Kola section salinity time-series $x(t)$, the estimated 9-year wavelet cycle $W_9(t)$, and the 9.3-year phase tide $u_{T/2}(t)$. In this time-series, the dominant 9-year wavelet cycle had an estimated phase

angle $\varphi_{T/2}(t) = (1.41-1.00)\pi$ (rad) in the period from 1960 to 2006. The correlation to the phase tide was estimated at $R_{T/2} = 0.20$ and $Q_{T/2} = 6.9$. This was the same phase as estimated in the 9-year temperature cycle.

The 9-year cycle was poorly correlated to the 9.3-year astronomic cycle. When the 74-year cycle was in a positive state, the dominant cycle was closer to a 6-year cycle. The 9-year cycle was dominant in the period from 1970, when the 74-year cycle turned into a negative state.

The wavelet analysis of Kola section temperature series showed the same correlation to lunar nodal tidal cycles of 9.3, 18.6 and 74.4 years as identified in NAW. The optimum 18-year cycle had the same phase as the 18.6-year amplitude tide and a time delay of about 2 years behind the 18.6-year fluctuation in NAW. The 18-year cycle had a phase-reversal in about 1925, when there was a phase-reversal in NAW. The 9-year temperature fluctuation was correlated to the 9.3-year phase tide. The phase angle was about the same as the 9.3-year phase tide and about 2 years behind the 9-year fluctuation of NAW. This time lag explains the non-correlation between the time-series.

The Kola section salinity time-series had the same dominant cycles correlated to the 18.6-year amplitude tide and 9.3-year phase tide. The phase angle was about the same as identified in the Kola section water temperature. This close correlation between sea level, sea temperature and salinity may suggest that the long-term Atlantic inflow to the Barents Sea is influenced by the lunar nodal tides.

3.9. Summary of results

Table 1 shows the lunar nodal spectrum as identified in all analyzed time-series in the Faroe-Shetland Channel
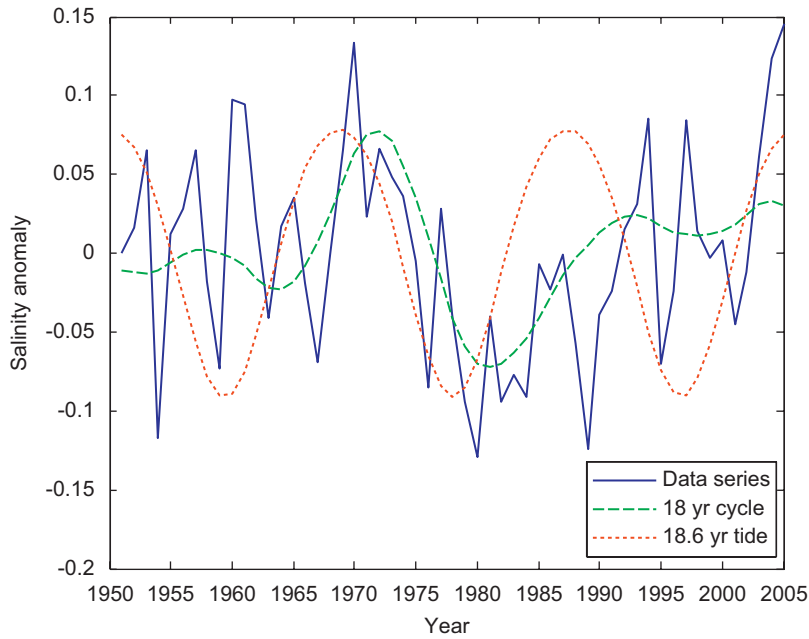
Fig. 14. Kola salinity anomaly, dominant 18-year wavelet cycle and 18.6-year amplitude tide.
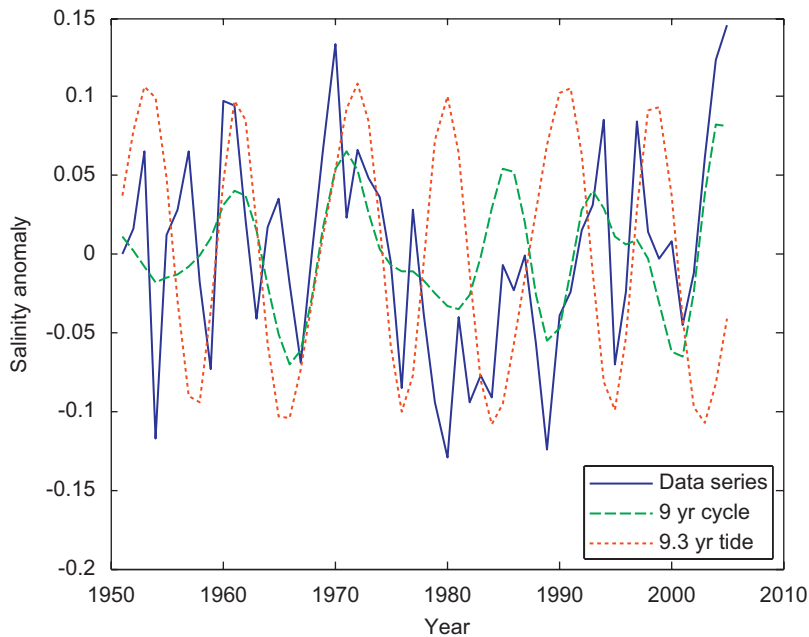
Fig. 15. Kola section salinity anomaly time-series, dominant 9-year wavelet and 9.3-year phase tide

and the Barents Sea. The correlation between dominant wavelet cycles and the lunar nodal spectrum is significant in all time-series except for the 9-year cycle in the Kola section salinity time-series. This confirms the hypothesis that the variability of the temperature and the salinity of NAW, MNAW and Barents Sea inflow water are correlated to the lunar nodal tide spectrum. The tidal fluctuations have stationary periods and temporary stable phase. The 18-year temperature cycles of NAW, MNAW and Kola section water had a phase-reversal when the 74-year cycle turned into a positive state in about 1925. The 18-year salinity cycle in NAW and MNAW had phase-reversal when the 74-year cycle has a polarity change in about 1925 and 1960.

Table 1
Summary of identified lunar nodal cycles in the various sea level and water property time-series

Time-series	Time (yr)	Nodal cycle (year)	Cycle phase, φ (rad)	Phase reversals, -1.0π (rad)	Correlation, R	Correlation quality, Q
Tide reference						
74.4 year tide		74.4	0.55π			
18.6 year tide		18.6	0.90π			
9.3 year tide		9.3	1.41π			
Faroe-Shetland						
Stockholm sea level	1774–2000	74.4	$(0.55-0.00)\pi$		0.39	3.1
Aberdeen sea level	1952–2003	18.6	$(0.90-0.10)\pi$		0.88	42
Aberdeen sea level	1952–2003	9.3	$(1.41-0.65)\pi$		0.39	3.1
NAW temperature	1895–2004	74.4	$(0.55-0.36)\pi$		0.93	27.8
NAW temperature	1895–2004	18.6	$(0.90-0.0/0.85)\pi$	1925	0.68	8.3
NAW temperature	1895–2004	9.3	$(1.41-0.65)\pi$		0.59	4.7
NAW salinity	1895–2004	74.4	$(0.55-0.26)\pi$		0.99	86
NAW salinity	1895–2004	18.6	$(0.90-0.0/1.00)\pi$	1925, 1960	0.82	75
NAW salinity	1895–2004	9.3	$(1.41-0.31)\pi$		0.41	45
MNAW temperature	1895–2004	74.4	$(0.29-0.05)\pi$		0.83	14.7
MNAW temperature	1895–2004	18.6	$(0.90-0.90)\pi$	1925	0.69	8.0
MNAW temperature	1895–2004	9.3	$(1.41-0.65)\pi$		0.51	5.9
MNAW salinity	1895–2004	74.4	$(0.55-0.36)\pi$		0.82	17.7
MNAW salinity	1895–2004	18.6	$(0.90-0.0/1.00)\pi$	1925, 1960	0.5	5.7
MNAW salinity	1895–2004	9.3	$(1.41-0.31)\pi$	1925, 1960	0.41	4.5
Barents Sea						
Murmansk sea level	1952–2003	18.6	$(0.90-0.20)\pi$		0.70	7.0
Murmansk sea level	1952–2003	9.3	$(1.41-0.90)\pi$		0.80	9.3
Kola temperature	1900–2005	74.4	$(0.55+0.71)\pi$		0.95	32.6
Kola temperature	1900–2005	18.6	$(0.90-1.2/0.2)\pi$	1925	0.77	10.0
Kola temperature	1920–2005	9.3	$(1.41-1.00)\pi$	1960	0.74	6.9
Kola salinity	1951–2005	18.6	$(0.90-0.30)\pi$		0.9	9.4
Kola salinity	1951–2005	9.3	$(1.41-1.00)\pi$		0.20	6.9

4. Discussion

The analysis was based on high-quality time-series, and wavelet analysis was used to identify single fluctuation periods and phase in time variant stochastic time-series. The wavelet method has limitations at the beginning and end of a time-series. A potential source of phase error exists from about 1900 to 1925, when the NAW time-series and the Kola time-series had some missing elements. Between these years, time-series gaps were filled using either cubic interpolation for the Faroe-Shetland time-series, or regression models for the Kola section temperature time-series. It is possible that the missing data have influenced the phase-reversal during this time. However, the phase-reversal in about 1925 is also found in the NAO winter index from 1864 and the annual mean rainfall in Norway (Yndestad, 2005, 2006).

The time-series of NAW and the Kola section are too short to allow for a good estimate of long-term cycles of about 74 years. However, the identification of the long-period cycles is confirmed in the longer Stockholm sea level time-series, as well as within longer Arctic time-series (Yndestad, 2006). It is, however, the similarities between the identified tidal-period cycles and their phase, compared to the period and phase of the astronomical cycles, in all investigated time-series that demonstrate the robust nature of wavelet analysis.

4.1. The forced tidal oscillation

Table 1 shows that the lunar nodal tide has a major influence on North Atlantic water property time-series variability. The 18-year lunar nodal tide, however, results in a variation of only 3–5% in the semi-diurnal tide. So why does this tide have such a major influence on temperature and salinity variability in Atlantic water properties in these northern areas? One answer may be that there is a fundamental difference between forced stationary long-term cycles and random short-term fluctuations. Small changes in stationary forced cycles have a major long-term influence on temperature variability when they are integrated over years in time and space. We may, then, understand long tides as forced oscillations on ocean systems.

Wavelet analysis identified the 18.6-year amplitude tide and the 9.3-year phase tide in the annual mean sea level time-series from Aberdeen and Murmansk. The cycle phase delay was estimated to be about 2 years, due to the transport delay. The 18.6-year amplitude tide has been known since Darwin (1880) and later from Loder and Garret (1978), Keeling and Whorf (1997), McKinnell and Crawford (2006) and other observations. Maksimov and Smirnov (1964, 1965, 1967) estimated the same lunar nodal tide period and phase in the Atlantic Ocean and Barents Sea and found the same cycle phase as in our study.

The unexpected observations made in the present study were the 9.3-phase tide and the 74.4-year sub-harmonic cycle, which are here identified for the first time in North Atlantic Water. The 74-year period has been identified in a number of long time-series. Schlesinger and Ramankutty (1994) analyzed the long-term temperatures from the Northern Hemisphere continental regions bounding the North Atlantic Ocean. In the North Atlantic region they found a dominant temperature cycle of about 76 years. Greenland ice cores showed periodic cycles of 20, 78, and 181 years; and temperature records from central England from 1700 to 1950 showed periodicities at cycles of 23 and 76 years (Borroughs, 1992; Currie, 1995). The period was also identified in polar movement, Arctic ice extent and the NAO winter index (Yndestad, 2006). A possible source of this periodic cycle may be related to the 75-year residence time for deep water in the Arctic Ocean (Bonisch and Schlosser, 1995).

4.2. Oceanic mixing processes

A possible mechanism directly linking the long-term tides to the oceanic thermohaline circulation in the North Atlantic and Nordic Seas is the role that oceanic tidal mixing may play in resupplying the potential energy required by the circulation (Munk and Wunsch, 1998; Wunsch 2000, Wunsch and Ferrari, 2004). The question then is how ocean tides dissipate their energies. Investigations by Egbert and Ray (2000) show that about 1 TW, or 25–30% of the total dissipation, occurs in the deep ocean. The estimated mixing energy required to maintain the large-scale thermohaline circulation is about 2 TW. One-half could therefore be provided by the tides.

The results presented in this paper suggest that our long-term hydrographic time-series provide evidence that tidal mixing may be an important mechanism influencing the properties—and perhaps the magnitude—of the thermohaline circulation. As Wunsch and Ferrari (2004) note, the budget of mechanical energy input to the ocean is not well understood, and the relevance of models that do not account for such energy sources and the resulting mixing they provide may be in doubt when used to predict the impact of future climate change on the Nordic Seas. The thermohaline circulation is a dynamic process, and interactions between the forced tidal process and the delayed process may influence the cycle phase by interference. The present analysis suggests that the temperature and salinity fluctuations in North Atlantic Water are influenced by tidal mixing, containing lunar nodal harmonics, before the water reaches the Faroe-Shetland Cannel. In these processes, the forced tidal energy is distributed as a coupled lunar nodal sub-harmonic spectrum in the thermohaline circulation. The identified 2-year phase delay between the Faroe-Shetland Channel and the Kola section may have an advective cause and thus supports the estimate from Helland-Hansen and Nansen (1909) and others.

Wavelet analysis of the oceanographic data series showed that there was no linear relationship between the 18.6-year amplitude tide and the identified 18-year temperature fluctuations. The 18-year temperature cycle in North Atlantic Water and in the Barents Sea had phase reversals in about 1925. Phase reversals are well known in physical and communication systems. In relation to the 18.6-year tide, a phase reversal was identified by Currie (1987, 1995) in long Nile records and Mazzerella and Palumbo (1994) in atmospheric pressure and the NAO winter index (Yndestad, 2006). The physical mechanism behind this phase reversal is unclear. Phase reversals can arise in forced oscillating non-linear systems (Stoker, 1950; Strogatz, 2000) This investigation showed that the phase reversal was associated with the 74-year sub-harmonic cycle. A possible explanation is interference in the mixing processes between the forced lunar nodal tides and non-linear feedback systems in the Atlantic Ocean. This situation may be modeled by the simple model $x(t) = A\sin(\omega_T t + 0.9\pi) + B \times \sin(\omega_{4T} t + 0.29\pi)$, where A represents the 18.6-year tide amplitude and B the 74-year tide amplitude. In this model, the 18.6-year tide will have a phase reversal when $B \gg A$. Harmonics from the 74-year cycle may then introduce temporary phase reversals in the 18.6-year tidal inflow of NAW in a manner that is dependent on the accumulated amplitude. The salinity had a mixing process from a different source. In this case, the mixing was correlated with the modulation process model $u_m(t) = -\sin(\omega_T t + 0.9\pi) \times \sin(\omega_T t/4 + 0.29\pi)$, which showed a more complex variability.

5. Conclusions

Wavelet analysis of some of the longest oceanographic time-series in the world indicated that the 18.6-year lunar nodal amplitude tide and the 9.3-year phase tide may influence the variability of temperature, salinity and sea level in the Faroe-Shetland Channel and the Barents Sea. The time-series had a mean variability correlated to the sub-harmonic cycle of about 74 years and an advective delay to the Barents Sea of about 2 years. The correlation between the lunar nodal tides and the ocean temperature variability indicated that deterministic lunar nodal tides may provide an important regional climate indicator that should be taken into account in forecasts of future regional climate change.

A possible explanation for the link between ocean climate indicators and the nodal tide is that energy from the forced lunar nodal tide may modify the Atlantic and Arctic thermohaline circulation systems through the input of mechanical energy via tidal mixing at topographic boundaries. The mixing processes influence long-term mean fluctuations and introduce phase reversals by interference between cycle periods.

References

Bochkov, Yu.A., 1982. Water temperature in the 0–200 m layer in the Kola-Meridian section in the Barents Sea, 1900–1981. Sb. Nauchn. Trud. PINRO, Murmansk 46, 113–122 (in Russian).

Bonisch, G., Schlosser, P., 1995. Deep water formation and exchange rates in the Greenland/Norwegian Seas and the Eurasian Basin of the Arctic Ocean derived from tracer balances. Progress in Oceanography 35, 29–52.

Boon, J.D., 2004. Secrets of the Tide. Horwood Publishing. ISBN 1-904275-17-6.

Borroughs, W.J., 1992. Weather Cycles Real or Imaginary? Cambridge University Press.

Currie, R.G., 1987. Examples and implications of 18.6- and 11-year terms in world weather records, Chap. 22, pp. 378–403. In: Rampino, M.R., Sanders, J.E., Newman, W.S., Konigsson, L.K. (Eds.), Climate: History, Periodicity, and Predictability: International Symposium Held at Barnard College, Columbia University, New York, New York, 21–23 May 1984 (R.W. Fairbridge Festschrift), Van Nostrand Reinhold Publishing Corp., New York, NY, 588pp.

Currie, R.G., 1995. Variance contribution of M_n and S_c signals to Nile river data over a 30–8 year bandwith. Journal of Coastal Research Special Issue No. 17. Holocene Cycles: Climate, Sea Levels and Sedimentation, pp 29–38.

Darwin, G.H., 1880. On the secular change of the orbit of a satellite revolving about a tidally distorted planet. Philosophical Transactions of the Royal Society of London 171, 713–891.

Daubechies, I., 1992. Ten lectures of wavelet. SIAM Journal on Mathematical Analysis 24, 499–519.

Daly, F., Hand, D.J., Jones, M.C., Lunn, A.D., MaConway, 1995. Elements of Statistics. Addison-Wesley Publishing Company. ISBN:0-201-42278-6.

Egbert, G.D., Ray, R.D., 2000. Significant dissipation of tidal energy in the deep ocean from ocean inferred from satellite alitimeter data. Nature 405 (6788), 775–778.

Ekman, M., 1999. Climate changes detected through the world's longest sea level series. Global and Planetary Change 21, 215–224.

Ekman, M., 2003. The World's Longest Sea Level Series and a Winter Oscillation Index for Norteren Europe 1774–2000. Small Publications in Historical Geophysics. No. 12. Summer Institute for Historical Geophysics Åland Islands.

Helland-Hansen, B., Nansen, F., 1909. The Norwegian Sea: its physical oceanography based on Norwegian researches 1900–1904. Report on Norwegian Fishery and Marine Investigations, vol. 2. Bergen, Norway, 390pp.+25 plates.

Izhevskii, G.K., 1961. Oceanological Principles as Related to the Fishery Productivity of the Seas. Pishcepromizdat, Moscow, [Transl. 1964: Israel Progr. Sci. Transl., Jerusalem]. 186pp.

Izhevskii, G.K., 1964. Forecasting of Oceanological Conditions and the Reproduction of Commercial Fish. Moscow: Pishcepromizdat. [Transl. 1966: Israel Progr. Sci. Transl., Jerusalem]. 95pp.

Keeling, C.D., Whorf, T.P., 1997. Possible forcing global temperature by oceanic tides. Proceedings of the National Academy of Sciences of the United States of America 94, 8321–8328.

Loder, J.W., Garret, C., 1978. The 18.6-year cycle of the sea surface temperature in the shallow seas due to tidal mixing. Journal of Geophysical Research 83, 1967–1970.

Loeng, H., 1989. The influence of temperature on some fish population parameters in the Barents Sea. Journal of Northwest Atlantic Fishery Science 9, 103–113.

Loeng, H., Bjoerke, H., Ottersen, G., 1995. Larval fish growth in the Barents Sea. In: Beamish, R.J. (Ed.), Canadian Special Publications of Fisheries and Aquatic Sciences, vol. 121. Climate Change and Northern Fish Populations, pp. 691–698.

Maksimov, I.V., Smirnov, N.P., 1964. Long range forecasting of secular changes of the general ice formation of the Barents Sea by the harmonic component method. Murmansk Polar Science Research Institute, Sea Fisheries 4, 75–87.

Maksimov, I.V., Smirnov, N.P., 1965. A contribution to the study of causes of long-period variations in the activity of the Gulf Stream. Oceanology 5, 15–24.

Maksimov, I.V., Smirnov, N.P., 1967. A long-term circumpolar tide and its significance for the circulation of ocean and atmosphere. Oceanology 7, 173–178 (English edition).

Matlab, 1997. Matlab. Wavelet Toolbox. Users Guide. The Math Works Inc.

Mazzerella, A., Palumbo, A., 1994. The lunar induced-signal in climatic and oceanic data over the Western Mediterranian Area and on its bistable phaing. Theoretical and Applied Climatology 50, 93–102.

McKinnell, S.M., Crawford, W.R., 2006. The 18.6-year lunar nodal cycle and surface temperature variability in the northeast Pacific. Journal of Geophysical Research 112 (C2).

Munk, W., Wunsch, C., 1998. Abyssal recipes II: energetics of tidal and wind mixing. Deep-Sea Research (Part I) 45 (12), 1977–2010.

Ottersen, G., Loeng, H., Raknes, A., 1994. Influence of temperature variability on recruitment of cod in the Barents Sea. ICES Marine Science Symposia 198, 471–481.

Ottersen, G., Ådlandsvik, B., Loeng, H., 2000. Predicting the temperature of the Barents Sea. Fishes in Oceanography 9 (2), 121–135.

Pugh, D.T., 1996. Tides, Surges and Mean Sea-level. Wiley, New York.

Schlesinger, M.E., Ramankutty, N., 1994. An oscillation in the global climate system of period 65–70 years. Nature 367, 723–726.

Stoker, J.J., 1950. Non-linear Vibrations in Mechanical and Electrical Systems. Interscience, New York.

Strogatz, S.H., 2000. Nonlinear Dynamics and Chaos. Westview Press. ISBN:0-7382-0453-6.

Tereshchenko, V.V., 1997. Seasonal and Year-to-Year Variation in Temperature and Salinity of the Main Currents along the Kola Section in the Barents Sea. PINRO Publ., Murmansk, 71pp. (in Russian).

Trofimov, A.G., 2000. Numerical Modelling of Water Circulation in the Barents Sea. PINRO Publ., Murmansk, 42pp. (in Russian).

Turrell, W.R., Slesser, G., Adams, R.D., Payne, R., Gillibrand, P.A., 1999. Decadal variability in the composition of Faroe Shetland Channel Bottom Water. Deep-Sea Research I 46, 1–25.

von Storch, H., Zwiers, F.W., 1999. Statistical Analysis in Climate Research. Cambridge University Press. ISBN:0-521-01230-9.

Wunsch, C., 2000. Moon, tides and climate. Nature 405 (6788), 743.

Wunsch, C., Ferrari, R., 2004. Vertical mixing, energy, and the general circulation of the oceans. Annual Review of Fluid Mechanics 36, 281–314.

Yndestad, H., 1999. Earth nutation influence on the temperature regime of the Barents Sea. ICES Journal of Marine Science 56, 381–387.

Yndestad, H., 2003. The code of long-term biomass cycles in the Barents Sea. ICES Journal of Marine Science 60, 1251–1264.

Yndestad, H., 2005. Prognoser for tilsig til vannkraft. HiÅ-Rapport 2005/01. Aalesund University College, Aalesund, Norway (in Norwegian).

Yndestad, H., 2006. The influence of the nodal cycle on Arctic climate. ICES Journal of Marine Science 63, 401–420.